JOURNAL OF APPLIED ELECTROCHEMISTRY 18 (1988) 601–607

Behavior of the corrosion potential and corrosion current of Cu–Ni alloys under erosion corrosion conditions. Effect of oxygen

PIERRE R. ROBERGE, RÉJEAN BEAUDOIN

Department of Chemistry and Chemical Engineering, Royal Military College of Canada, Kingston, Ontario K7K 5L0, Canada

Received 5 October 1987; revised 27 January 1988

Electrochemical impedance spectroscopy has been used as an erosion corrosion rate-monitoring technique. The Cu–Ni alloys used for this study were machined into cylinders and submitted to high speed rotation in a sodium chloride solution after an initial passivation period. The hydrodynamic behavior of the liquid environment on these rotating surfaces was analyzed and related to other geometries and conditions. Breakdown of the outer passivation film by erosion was easily observed for the 90–10 Cu–Ni alloy and for two 70–30 Cu–Ni alloys. A comparison of I_{corr} with the values of the free E_{corr} clearly indicated a time lag between those two components. This can best be explained by the existence of a concentration gradient of oxygen throughout the film thickness. The time domain of these phenomena is also indicative of solid state equilibrium.

1. Introduction

Copper–nickel alloys are used for piping in many commercial ships and warships, and for heat exchangers in power plants cooled by sea water [1]. These corrosion-resistant alloys are protected by the formation of a surface film in sea water. The role of this film in reducing corrosion is unclear; however, the corrosion product of 90–10 Cu–Ni is known to consist of a loosely adherent porous layered structure consisting primarily of cupric hydroxychloride over a thin tightly adherent layer of cuprous oxide [2–5]. Until recently, Cu–Ni was believed to get its corrosion resistance from the inner cuprous oxide layer acting as a p-type semiconductor [4, 5]. More recently, Kato *et al.* [2, 6] have developed the following mechanistic model: an inner cuprous oxide layer provides a diffusion barrier to the cathodic reaction while it is also a poor catalyst for the oxygen reduction reaction. Hack *et al.* [1] also showed that the outer, loosely adherent, corrosion product layer must limit the corrosion rate, the rate being limited by the poor catalytic nature of the corrosion product surface for the oxygen reduction reaction.

For critical marine applications consideration was given to finding alloys with higher strength and greater resistance to erosion corrosion. This would allow the reduction of the total weight of a system by utilizing higher velocity sea water [7]. The behavior of Cu–Ni alloys has been studied under flow conditions and with oxygen concentration as a variable, mainly because of its importance during shutdown of systems. Previous observations of Cu–Ni alloys submitted to erosion conditions indicated, from the time involved in the phenomenon, that diffusion of molecular oxygen and of ionic species was taking place in the solid state.

A simple experimental set-up based on electrochemical impedance measurements has been designed to simultaneously observe the corrosion potential and the corrosion current of a prepassivated alloy under flow conditions.

2. Experimental details

Three alloys were used in this study: a 70–30 Cu–Ni modified with niobium, a 70–30 Cu–Ni modified with chromium and a 90–10 Cu–Ni, all three alloys being satisfactory for sea-water piping systems. Their chemical composition is given in Table 1.

The specimens were machined from cast sample in cylindrical shapes having a diameter of 1.2 cm and a height of 2.6 cm making a total exposed surface of 10^2 cm. The cylindrical specimens were polished to 500 grit, then washed with a good degreasing agent, methylene chloride, with fresh reagent grade acetone and then with double distilled water. This pretreatment procedure is similar to the method proposed by Dobb *et al.* [8]. The samples were immersed in saline solution for a period of 10 days. Macdonald *et al.* [9] have shown that the corrosion potential reaches a stable value after 5 days, indicating a steady state in the film formation.

The one-compartment cell was a closed 2-l beaker containing 1 l of electrolyte. The 3% NaCl solution was made up with double distilled water and ACS grade NaCl. The cell was left at room temperature (21° C) and purged with air or with a mixture of air and nitrogen to obtain the required molecular oxygen concentration in solution. The oxygen concentration in solution was monitored using an oxygen selective electrode (Orion Research, Model 97-09-00).

The electrochemical impedance measurements were

0021-891X/88 $03.00 + .12

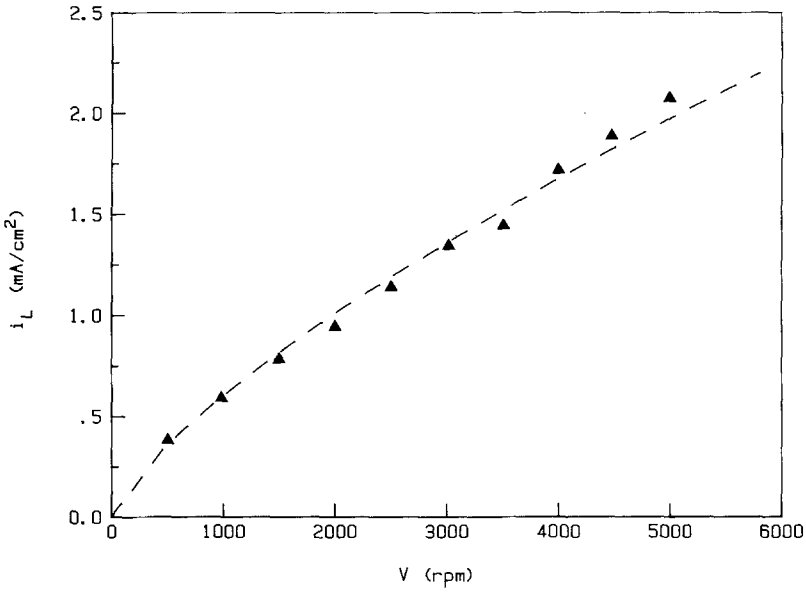

Fig. 1. Oxygen reduction limiting current density on a pure copper cylinder as a function of rotation speed. Experimental points and curve generated from Equation 1.

made with an AC generator/analyser (Solartron model 1250) controlled by a Hewlett–Packard model HP85 microcomputer. The sample was screwed into the rotating assembly (Pine Instrument Company) and the measurements were made at 0 rpm (without rotation) and at 5000 rpm. The AC measurements were made in two ways: the first was in a potentiostatic mode (Solartron model 1186) with a three-electrode cell. In the second mode the corrosion potential was left floating and a two-electrode cell was used following a technique described elsewhere [10]. Two high surface area carbon electrodes were used as counter electrodes in order to minimize their impedance contribution in the second mode of operation. The corrosion potential was measured between the Cu–Ni cylinders and a saturated calomel reference electrode (SCE) with an IEEE controllable multimeter.

The hydrodynamic conditions for this cell geometry were characterized by measuring the mass transfer limiting current density (MTLCD) of oxygen reduction at different rotation speeds on a similarly machined pure copper cylinder. This technique was originally described by Ponzano *et al.* [11]. The MTLCD (i_L) for a rotating cylinder of diameter d can be expressed by Equation 1 where ν = kinematic viscosity, z = number of exchanged electrons, C_0 = oxygen concentration at the interface, F = Faraday constant, Re = Reynolds number, Sc = Schmidt number.

$$i_L = 0.0791 \frac{\nu z F C_0}{d} \mathrm{Re}^{0.7} \mathrm{Sc}^{-0.644} \quad (1)$$

The MTLCD for a tube shape is obtained from Equation 2.

$$i_L = 0.0396 \frac{\nu z F C_0}{d} \mathrm{Re}^{0.755} \mathrm{Sc}^{-0.67} \quad (2)$$

From Equations 1 and 2 it is found that a rotation speed of 5000 rpm applied to the cylinders previously described would thus correspond to an average seawater velocity of 3.75 m s^{-1} in a tube having a diameter of 2.5 cm. Figure 1 shows the MTLCD measured on a pure copper cylinder with the cell geometry used in this study.

Poulson summarized the hydrodynamic profiles for various specimen geometries [12]. He also evaluated the transition between turbulent and laminar flows for each geometry. Such considerations are important when choosing a geometry to simulate specific hydrodynamic conditions.

Table 1. Analysed chemical composition of the alloys

	90/10	*70/30–Nb*	*70/30–Cr*
Cu	88.12	67.7	65.7
Ni	10.35	29.3	30.78
Fe	0.59	1.0	0.77
Mn	–	0.81	0.75
Si	0.25	0.2	0.31
Nb	0.04	0.42	–
C	0.002	0.005	0.05
Mg	0.012	–	–
Cr	–	–	2.1
S	–	–	0.006
Ti	–	–	0.06
P	–	–	0.005

3. Results

The electrochemical impedance diagrams measured with the potentiostat manually set at the corrosion potential (E_{corr}) and with the two-electrode assembly can be superimposed with the advantage that the second configuration leaves the specimen at its free E_{corr}. It then becomes possible to measure the impedance diagrams and the free E_{corr} almost simultaneously.

From the RC model of an electrochemical interface it is known that the intercept on the real axis, at low frequencies, is a measure of the polarization resistance (R_p) of the alloy [1]. Corrosion rates can be related to the reciprocal of this R_p with the Stearn–Geary low overvoltage approximation of the Butler–Volmer equation. Macdonald *et al.* [9] have shown excellent

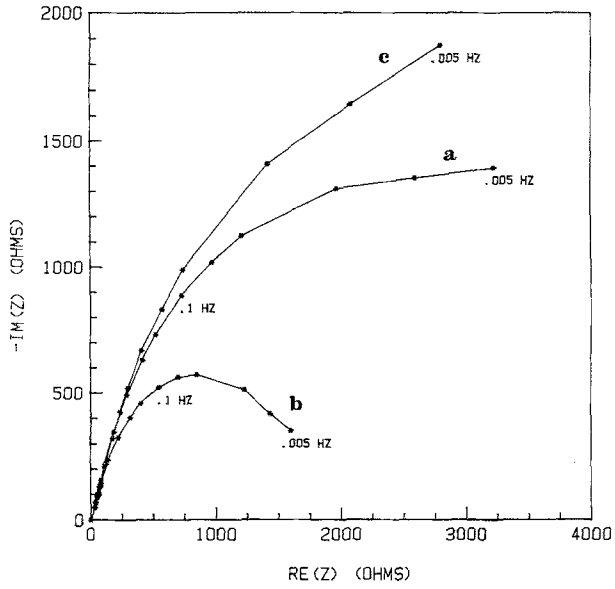

Fig. 2. Impedance diagrams made on a 10-day passivated 70–30 Cu–Ni alloy containing niobium (a) in a quiescent condition; (b) after 8 h of rotation at 5000 rpm; (c) in a quiescent condition 16 h after the rotation period.

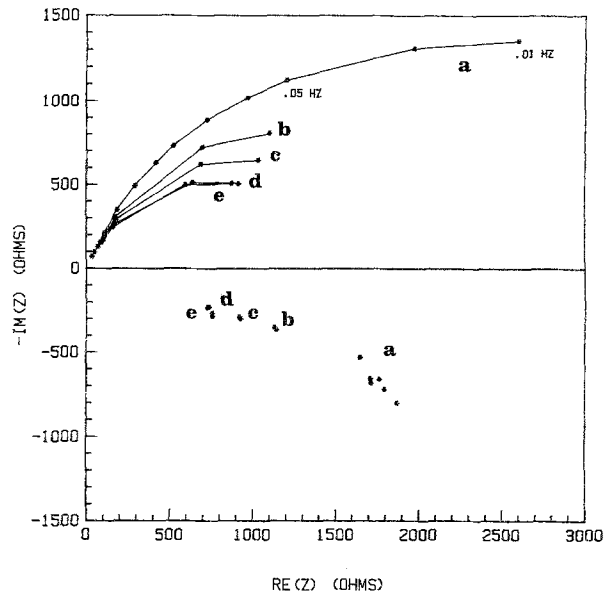

Fig. 3. Evolution of the impedance diagrams and of the projected centres for a 10-day passivated 70–30 Cu–Ni cylinder rotating at 5000 rpm: (a) complete diagrams in quiescent condition; (b), (c), (d) and (e) diagrams made using four high frequency measurements after 30, 45, 150 and 300 min of rotation at 5000 rpm.

agreement between such calculated corrosion rates and directly measured weight losses for Cu–Ni alloys in sea water.

Figure 2 shows the impedance diagrams obtained with the 70–30 Cu–Ni alloys containing niobium in three equilibrium conditions. With such curves R_p cannot obviously be obtained directly from the low frequency intercept with the real axis but has to be extrapolated. Extrapolations from admittance diagrams or from projection of common centres formed by three successive points on the impedance diagrams [13] have led to R_p. Figure 3 shows the evolution of the impedance behavior when the sample is submitted to a rotation speed of 5000 rpm and Table 2 gives a comparison of R_p calculated with the two techniques. Quick measurements have been made using only four selected frequencies and R_p was evaluated from the apparent diameters of the semicircles [13]. The fact that these centres are found below the real axis is generally attributed to the surface heterogeneity caused by a distribution of the reaction rate with location on the electrode surface [15]. Such a phenomenon is common with passivated alloys.

Figure 4 illustrates the diagrams obtained with the 90–10 Cu–Ni alloy both in quiescent condition and at a rotation speed of 5000 rpm. The high frequency part of the diagram forms a semicircle whereas the low frequency part gives almost a straight line which may be attributed to the beginning of a huge second semicircle or to the presence of a Warburg component. The diameter of this hypothetical semicircle would be very large and cannot be related to R_p or to the usual corrosion rates observed for this type of alloy in sea water. However, the semicircles formed by extrapolating the high frequency part of these diagrams led to more realistic R_p and corrosion rates.

Figure 5 shows the impedance diagrams obtained with the 70–30 Cu–Ni alloy containing chromium in three equilibrium conditions. As previously observed for the other alloys, the low frequency part of the diagrams obtained in quiescent condition does not fall into a semicircular pattern. However, the diagrams taken under rotating conditions give a clear semicircle from which R_p is easily obtained.

Table 2. Polarization resistance extrapolated from the admittance diagram and from the centres formed by three points shown in Fig. 2

	Curve					
	a	a[1]	b	c	d	e
Time (h)	0	0.25	0.50	0.75	2.5	5.0
Condition (rpm)	0	5000	5000	5000	5000	5000
Centres ± 5% (kohms cm^2)	35	35	22.5	19.0	15.0	15.5
Admittance ± 5% (kohms cm^2)	37	37	24	19.0	15.5	15.0

(a[1] is superimposed on a).

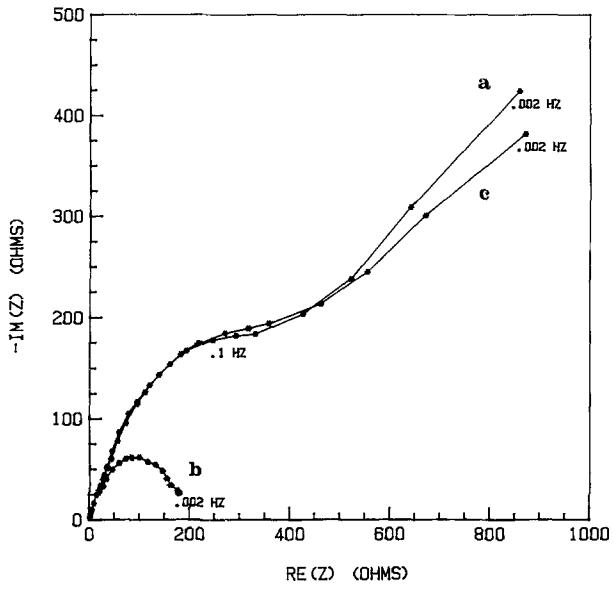

Fig. 4. Impedance diagrams for a 10-day passivated 90–10 Cu–Ni alloy: (a) in a quiescent condition, (b) after 8 h at a rotation speed of 5000 rpm, (c) quiescent, 16 h after stopping the rotation.

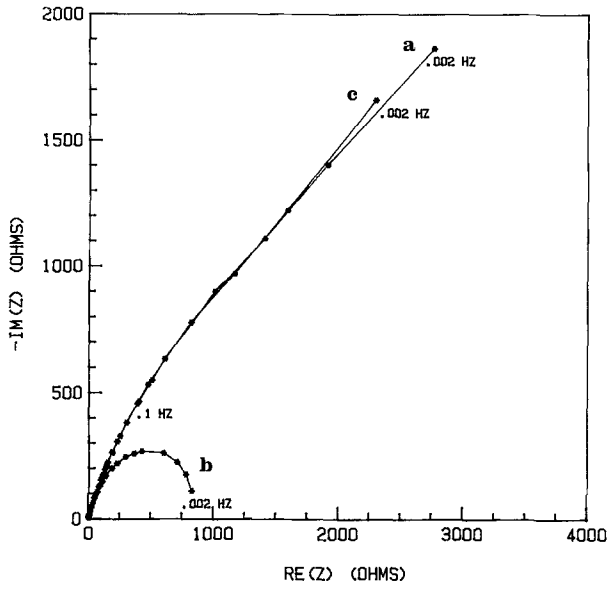

Fig. 5. Impedance diagrams made on a 10-day passivated 70–30 Cu–Ni alloy containing chromium: (a) in a quiescent condition; (b) after 8 h of rotation at 5000 rpm; (c) in a quiescent condition 16 h after the rotation period.

4. Discussion

The kinetics of the corrosion reactions can best be explained with the help of the Evans' diagram shown in Fig. 6 [16]. The cathodic reaction

$$\text{cathode } \tfrac{1}{2}[O_2] + [H_2O] + 2e \rightleftharpoons 2[OH^-] \quad (3)$$

supplying the adsorbed oxygen is represented by line AB. The anodic reaction

$$\text{anode } 2Cu \rightleftharpoons 2Cu^+_{sol} + 2e^- \quad (4)$$

which would take place in the absence of passivation is represented by line CD. Shortly after immersion into aerated sea water, a Cu–Ni alloy forms a protective layer of corrosion products

$$2Cu^+_{sol} + 2[OH^-] \rightleftharpoons Cu_2O + [H_2O] \quad (5)$$

with an associated IR drop that causes the slope, or resistance, to increase from the value given by line CD to the value given by lines T_n. The intersection of lines T_n and AB gives the corrosion potential E_{corr} and the corrosion current I_{corr}. Eventually, the IR drop becomes large enough so that E_{corr} reaches $E_{Cu_2O/Cu_2(OH)_3Cl}$.

$$2[Cu^{2+}_{sol}] + 3[OH^-] + Cl^- \rightleftharpoons Cu_2(OH)_3Cl \quad (6)$$

At this point the outer corrosion product layer of $Cu_2(OH)_3Cl$ forms [3]. The behavior of Cu–Ni alloys under flow conditions can also be explained with this model. Under erosion conditions the following phenomena occur. At first, the film is eroded by moving solution and dissolution of the outer porous layer [3] occurs, shifting Equation 6 to the right. On the Evans' diagram this corresponds to a shift from point 1 to point 2. During a second phase, the oxygen reduction reaction rate increases from point 2 to point

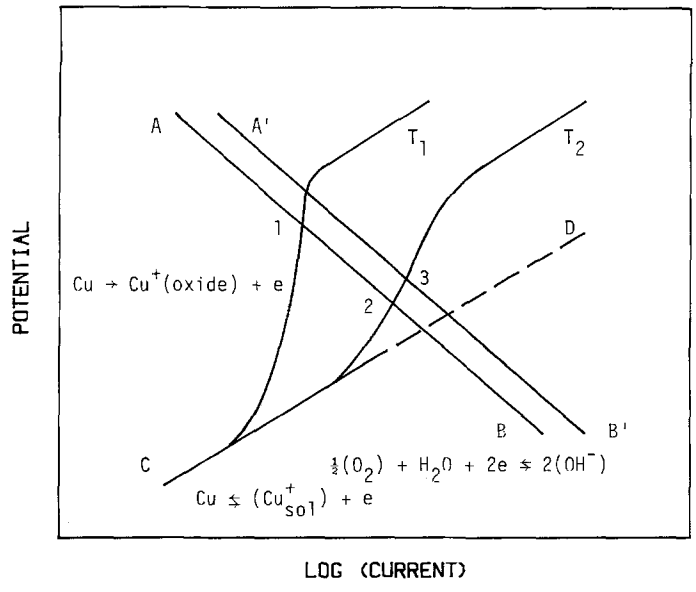

Fig. 6. Evans' diagram illustration of the corrosion behavior with time (time T_2, time T_1) of Cu–Ni alloys in aerated sea water [16].

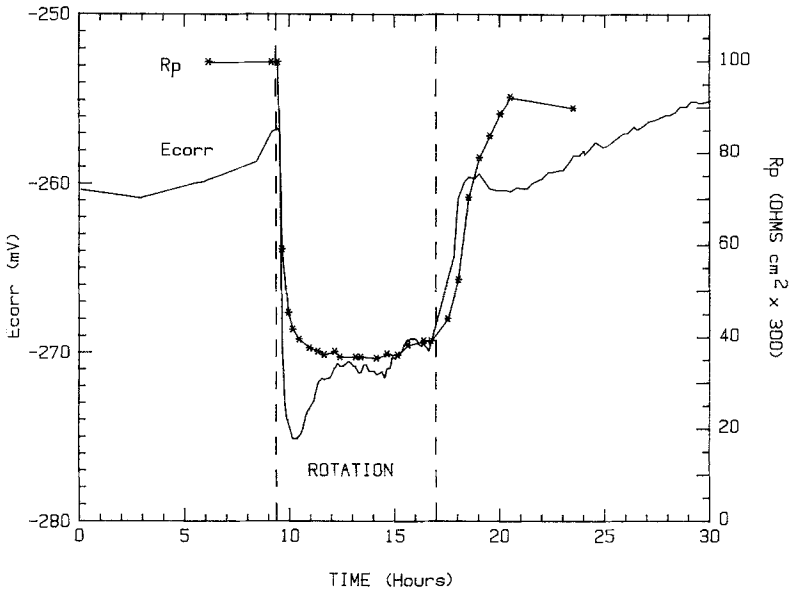

Fig. 7. Behavior of E_{corr} and R_p with time and rotation (5000 rpm) for a 10-day passivated 70–30 Cu–Ni alloy in an air-saturated solution ($[O_2]$ = 6.3 ppm).

3. However, this cathodic reaction has been proved to be independent of rotation speed [6].

Figure 7 shows the evolution of E_{corr} and of R_p for the 70–30 Cu–Ni containing niobium in an air-saturated solution. Immediately after starting the rotation, E_{corr} goes toward more negative values, reaching a minimum after 30 min and a stable value after 2 h. R_p also decreases rapidly but levels off at its minimum value after 2 h. Both R_p and free E_{corr} recover their original values when the rotation is stopped. This behavior can be explained by a lag in the increase of the rate of oxygen reduction (a shift from point 1 to point 2 and then to point 3 on the Evans' diagram) caused by the solid state nature of the reacting oxygen. The whole time involved in those processes, approximately 2 h, is also indicative of changes happening in solid state conditions.

Figure 8 illustrates a similar behavior for a solution slightly depleted in oxygen (4.5 ppm O_2) except for the longer time necessary to reach a new equilibrium. For a more severe depletion in oxygen (3.5 ppm O_2), illustrated in Fig. 9, E_{corr} and R_p behave differently. In this case E_{corr} drops slowly to more negative values when the rotation is started and returns slowly toward positive potentials when it is stopped. In this case, the changes in R_p are also very slow during its decrease, the transitory shift in E_{corr} has disappeared and the recovery of the original values, when the rotation is stopped, takes a very long time (4 h). The slower reformation of the passive film indicates that the concentration of oxygen in solution is close to becoming critical for the stability of this type of passivation film.

In fact, the results at 1.0 ppm of oxygen presented in Fig. 10 show a transition in the behavior of E_{corr}. It is unusually shifted toward more positive values. It is also shifted in the negative direction when the rotation is stopped. On the Evans' diagram this corresponds to a displacement of line AB. The corrosion current is increased in the usual way.

This behavior confirms the effect of the oxygen gradient inside the film. For a low oxygen concentration in solution, the corrosion reactions consume the

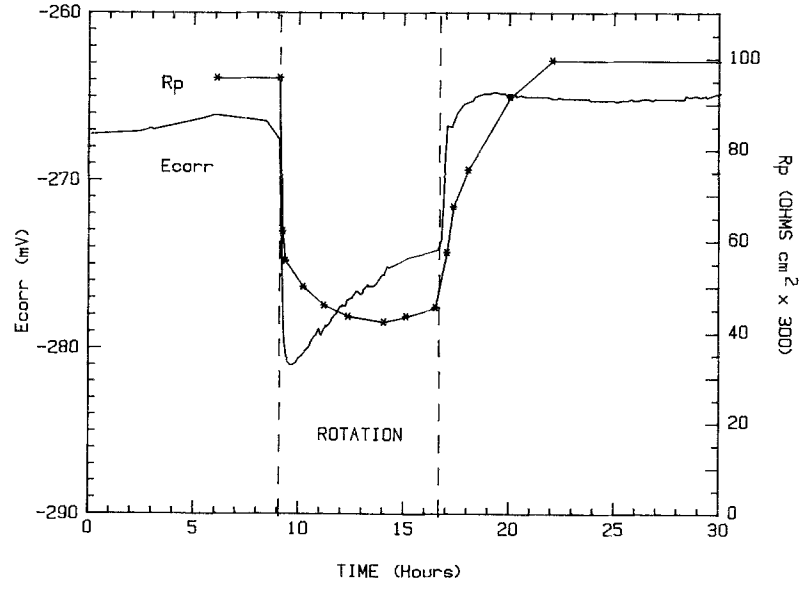

Fig. 8. Behavior of E_{corr} and R_p with time and rotation (5000 rpm) for a 10-day passivated 70–30 Cu–Ni alloy in an oxygen-depleted solution ($[O_2]$ = 4.5 ppm).

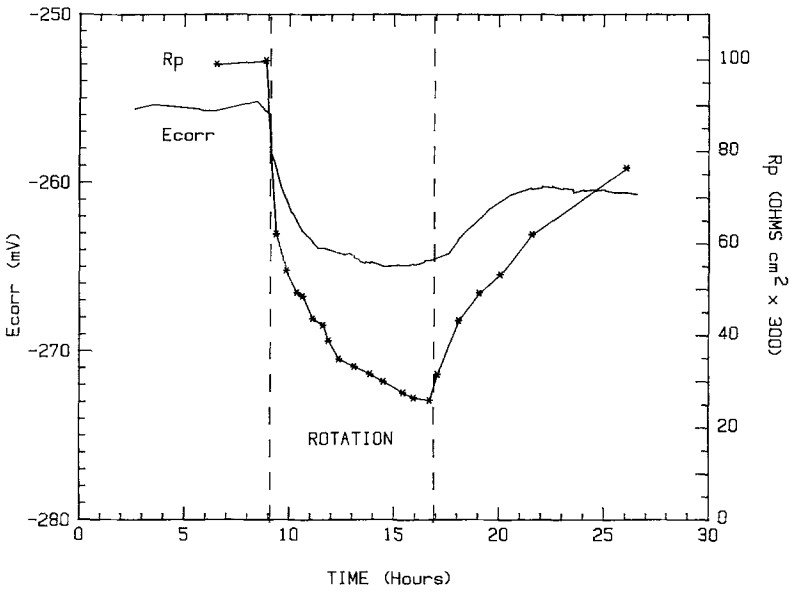

Fig. 9. Behavior of E_{corr} and R_p with time and rotation (5000 rpm) for a 10-day passivated 70–30 Cu–Ni alloy in an oxygen-depleted solution ($[O_2]$ = 3.5 ppm).

available oxygen and its concentration inside the film is almost zero. When rotation is started, it brings more oxygen to an eroded surface. This results in a positive shift in E_{corr} and an increase in I_{corr}. When the rotation is stopped, a depletion in oxygen due to the corrosion reaction causes E_{corr} to shift back toward negative values. Rotation in an air-saturated solution also caused a negative shift in E_{corr}. This was explained by a temporary deficiency in oxygen inside the film that was re-adjusted with time to an equilibrium concentration, bringing E_{corr} to its stable value only after two hours as shown in Fig. 7.

The passivity of Cu–Ni alloys also changes with time. A 76-day passivation period produces a higher R_p and the changes with rotation are slower and in parallel with E_{corr}. The lag in R_p versus E_{corr} is nearly absent in this case. However, R_p is much higher and E_{corr} is more positive than for a 10-day old film.

The 90–10 Cu–Ni behavior under erosion conditions, illustrated in Fig. 11, indicates a reduction in R_p faster than the negative shift in corrosion potential. The lag between R_p and E_{corr} is absent in this case. When the rotation is stopped, the recovery of R_p is, however, slower than the changes in E_{corr}. This corresponds to a direct shift from point 1 to point 3 on the Evans' diagram. The recovery toward equilibrium, when the rotation is stopped, is, however, different in this case. E_{corr} reaches its equilibrium value in a short time but R_p increases very slowly, probably due to a slow thickening of the passive film.

Kato *et al.* [6] and Hack *et al.* [1] compared these types of alloys with pure copper and concluded that most of the decrease in corrosion rate is due to a decrease in the rate of oxygen reduction. The good corrosion-resistant character of the Cu–Ni alloys in sea water is based on a low exchange current density for this reaction. Hack *et al.* [1] demonstrated that removing the outer porous layer of the film or sputter-coating the film with palladium, a coating that promotes oxygen reduction, has a larger effect on the 70–30 Cu–Ni alloys than on the 90–10 alloys.

The results obtained with the 70–30 Cu–Ni alloy containing chromium, Fig. 12, show a parallel shift of E_{corr} and R_p that is not surprising if the appearance of

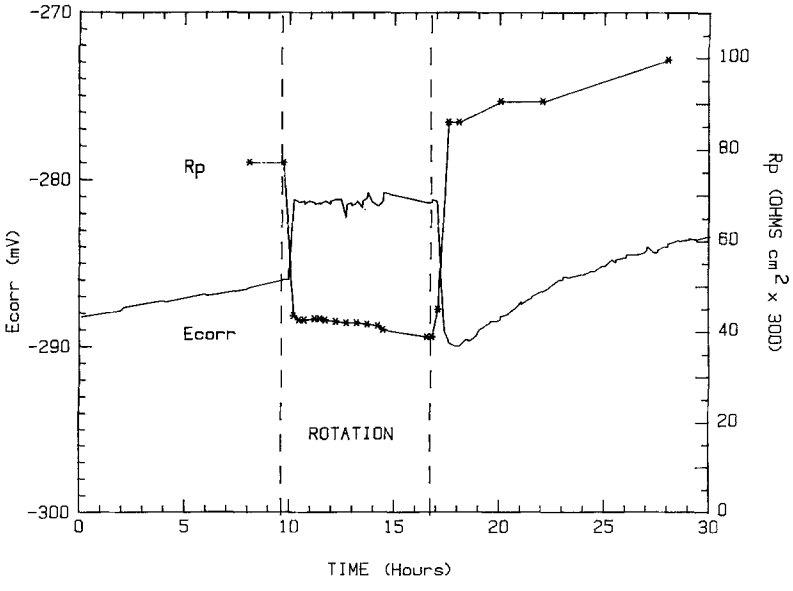

Fig. 10. Behavior of E_{corr} and R_p with time and rotation (5000 rpm) for a 10-day passivated 70–30 Cu–Ni alloy in an oxygen-depleted solution ($[O_2]$ = 1.0 ppm).

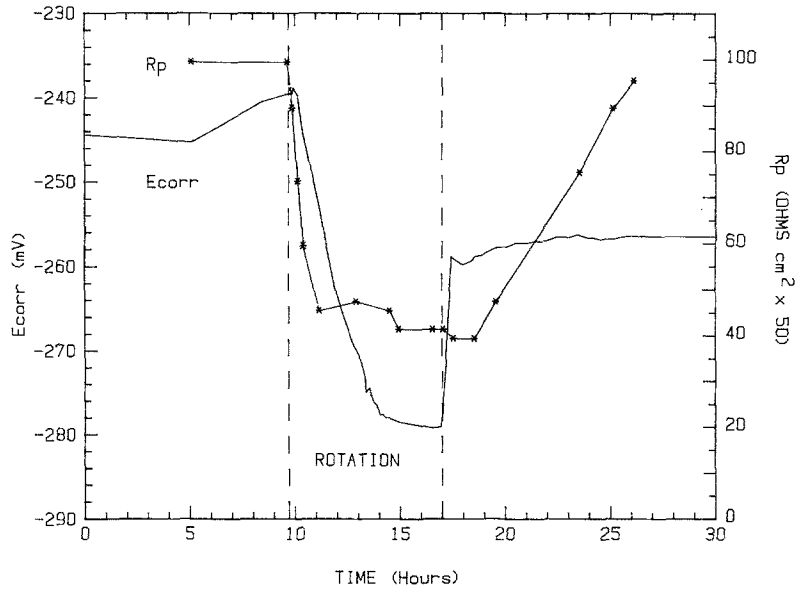

Fig. 11. Behavior of E_{corr} and R_p with time and rotation for a 10-day passivated 90–10 Cu–Ni alloy in an air-saturated solution.

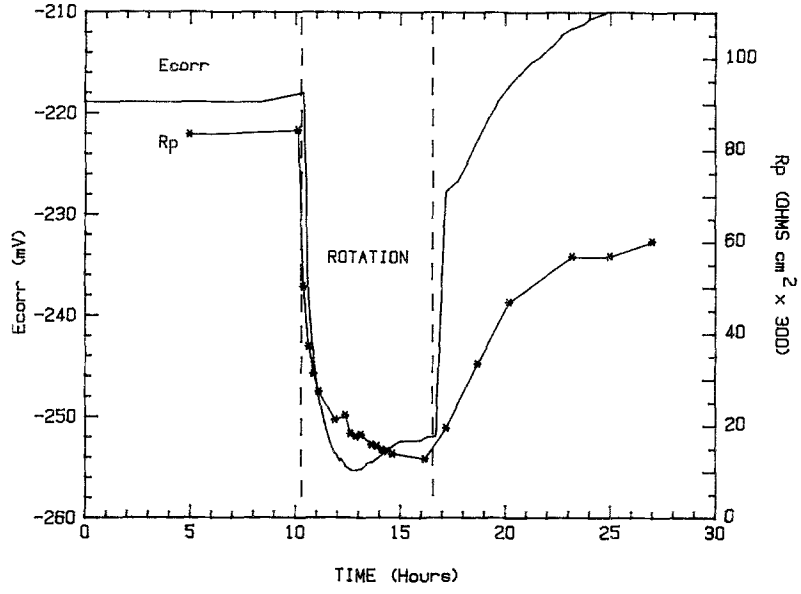

Fig. 12. Behavior of E_{corr} and R_p with time and rotation for a 10-day passivated 70–30 Cu–Ni alloy containing chromium in an air-saturated solution.

the alloy is considered. There is no significant corrosion product build-up as for the standard 70–30 Cu–Ni alloys. The surface of this alloy stays bright with the exception of a few tarnished spots, whereas the passivated Cu–Ni with niobium becomes green as is usual with Cu–Ni alloys in salt water [9]. The effect of eroding the surface is, in this case, immediately reflected in E_{corr} and R_p.

Acknowledgements

The support of this research by the Defence Research Establishment Atlantic is gratefully acknowledged. We are indebted to Dr R. S. Hollingshead and C. M. Hanham for helpful information concerning the marine applications and behaviors of the Cu–Ni alloys and to Dr M. Sahoo for providing them.

References

[1] H. Hack, H. Shih and H. Pickering, Proceedings Vol. 86-7, The Electrochemical Society Inc., San Diego, California (1986).

[2] C. Kato, B. G. Ateya, J. E. Castle and H. W. Pickering, *J. Electrochem. Soc.* **127** (1980) 1890.

[3] C. Kato, J. E. Castle, B. G. Ateya and H. W. Pickering, *J. Electrochem. Soc.* **127** (1980) 1897.

[4] R. F. North and M. J. Pryor, *Corros. Sci.* **10** (1970) 297.

[5] J. M. Popplewell, R. J. Hart and J. A. Ford, *Corros. Sci.* **13** (1973) 295.

[6] C. Kato and H. W. Pickering, *J. Electrochem. Soc.* **131** (1984) 1219.

[7] C. M. Hanham, M. Sahoo and R. S. Hollingshead, 1983 ASM Metals Congress, Philadelphia, Pennsylvania (1983).

[8] D. E. Dobb, J. P. Storvick and G. K. Pagenkopf, *Corros. Sci.* **26** (1986) 525.

[9] D. D. Macdonald, B. C. Syrett and S. S. Wing, *Corrosion* **34** (1978) 289.

[10] D. E. Williams and J. Asher, *Corros. Sci.* **24** (1984) 185.

[11] G. P. Ponzano, M. Bassoli and P. I. Bonora, *Werkst. Korros.* **27** (1976) 568.

[12] B. Poulson, *Corros. Sci.* **23** (1983) 391.

[13] P. R. Roberge and R. Beaudoin, Proceedings Vol. 86–7, Electrochemical Society Inc., San Diego, California (1986).

[14] L. Lemaitre, M. Moors and A. P. Van Peteghem, *J. Appl. Electrochem.* **13** (1983) 803.

[15] A. Bonnel, F. Dabosi, C. Deslouis, M. Duprat, M. Keddam and B. Tribollet, *J. Electrochem. Soc.* **130** (1983) 753.

[16] L. E. Eiselstein, B. C. Syrett, S. S. Wing and R. D. Caligiuri, *Corros. Sci.* **23** (1983) 223.